Journal of Thermal Analysis and Calorimetry, Vol. 67 (2002) 403–409

SOLID-STATE REACTIONS OF MERCURY WITH PURE NOBLE METALS
Part 2. Mercury–iridium system

F. L. Fertonani[*]*, E. Milaré, A. V. Benedetti and M. Ionashiro*

Instituto de Química, Universidade Estadual Paulista, Araraquara, São Paulo,
C.P. 355, CEP 14.801-970, Brazil

Abstract

Thermogravimetry, cyclic voltammetry and other analytical techniques were used to study the reactions of mercury with pure iridium. The results allowed to suggest when subjected to heat or anodic stripping voltammetry an electrodeposited mercury film reacts with Ir substrate and at least three mass loss steps and three peaks appear in the mercury desorption process. The first two were attributed to Hg(0) species removal like a mercury bulk and a mercury monolayer. The last can be ascribed to the mercury removal from a solid solution with iridium.

Keywords: cyclic voltammetry, iridium, mercury, SEM, TG, X-ray diffraction

Introduction

In recent works, pure platinum, rhodium and iridium, and alloys of platinum–iridium and platinum–rhodium have been widely used to prepare microelectrodes and ultra-microelectrodes [1–5], and catalysts used in petroleum cracking industry [6]. It is known that when solid metals are placed in contact with liquid metals, a variety of physicochemical changes may occur, e.g., complete or partial solution of the solid, intermetallic compounds formation at the liquid–solid interface or in the solution, grain boundary grooving, and liquid metal embrittlement. Such changes may also cause structural deterioration of the solid surface [2, 3, 5–7].

Considering the importance of the development of new substrates with high resistance to mercury amalgamation, $Pt–Ir_{(20\ mass\%)}$ has been suggested as an appropriate substrate for mercury deposition because its surface is not scarred by interaction with mercury [8]. However, intermetallic compounds such as $PtHg_4$ and $PtHg_2$ on the $Pt–Ir_{(20\ mass\%)}$ alloy surface were identified based on X-ray diffraction results [4]. The resulting changes in the surface morphology were investigated by optical interferometry and SEM, and the changes in the Hg-noble alloy interaction energy by XPS. XPS results were interpreted considering a model where the electrode/solution interphase

* Author for correspondence: E-mail: fertonan@iq.unesp.br

1418–2874/2002/ $ 5.00
© 2002 Akadémiai Kiadó, Budapest
Akadémiai Kiadó, Budapest
Kluwer Academic Publishers, Dordrecht

is composed by different phases including a three layered region structure, containing at least two Pt–Hg intermetallics: $PtHg_4$ and $PtHg_2$, and a substrate modified region, iridium rich [4].

Recently screen-printed Ir–Hg electrode had been prepared by sputtering deposition of iridium on silica wafer [9]. Iridium in this device was used because of its low solubility in mercury and its non-chemical surface interaction with mercury. However, it was observed when the stripping process to Hg removal is used the electrode surface area increases as a consequence of the mercury–iridium interactions that destabilize the electrode surface.

In the present work, films of mercury were electrodeposited on pure iridium foils and mercury desorption were investigated by TG/DTG and cyclic voltammetry. The new generated surfaces at the end of each mass loss step in the TG curve was studied using EDX, SEM, Surface Mapping and X-ray diffractometry.

Experimental

Pure iridium foils (80 mm^2) were polished with Al_2O_3 (particle size <0.3 μm) in aqueous suspension and washed in HNO_3: H_2O (50% v/v) using an ultrasonic bath.

All electrochemical measurements were performed using an ECOCHEMIE Potentiost-Galvanostat PGSTAT10 and a matrix exchange cell (10 mL) with: 1. Ir work electrode (64 mm^2); 2. a large platinum counter-electrode; 3. $Ag/AgCl,KNO_{3(sat)}$ as reference electrode; 4. a degassed solution containing 1.40 mmol Hg_2^{2+} +1.00 M KNO_3+HNO_3 (pH 1) and v=50 mV s^{-1}. Cyclic voltammograms were made: 1. for different cathodic switching potentials ($E_{\lambda c}$) between –0.20 V≤$E_{\lambda c}$≤0.20 V; 2. for $E_{\lambda c}$= –0.20 V and the reverse scan stopped at several potentials in the anodic region of peaks B and C. In each experiment, the anodic potential was held at a constant value until the current reached a null value and then the scan was restarted.

For TG experiments, Hg was electrodeposited on foils in a degassed solution containing 60.0 mmol Hg_2^{2+} +1.00 M KNO_3+HNO_3 (pH 1), at –0.46 V/ENH for 300 s in a stirred solution. TG curves were obtained from 30 to 800°C, at 5°C min^{-1} under a purified N_2 atmosphere (150 cm^3 min^{-1}), using a Mettler Thermoanalyser TA400 System.

The sample surfaces, before and after heating to various temperatures, were examined by JEOL JSM-T330A microscope coupled to a NORAN system to obtain SEM images and EDX microanalysis. The X-ray diffractograms were obtained with a SIEMENS D5000 diffractometer.

Results and discussions

Figure 1 shows TG and DTG curves for quenched pure iridium foil recorded from 30 to 800°C. Although the TG and DTG curves (Fig. 1a) indicate mass losses in one step between 30 and ca. 190°C, it can be pointed out that this process occurs in three consecutive steps. The first and second mass loss steps are consecutive and of fast kinetics (Fig. 1a), while the last step shows a very slow kinetics (Fig. 1b, detail expanded scale).

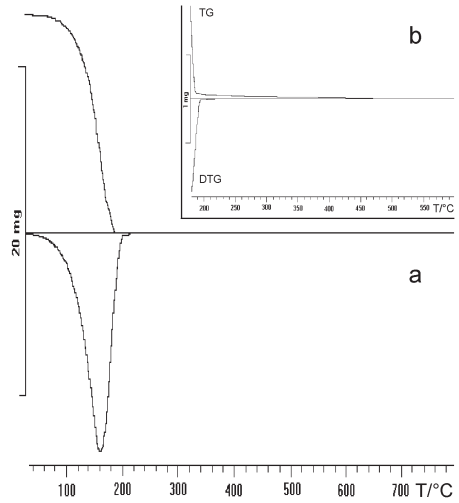

Fig. 1 a – TG and DTG curves for Ir foils containing electrodeposited mercury; b – magnification of the last step in the TG and DTG curves

The first mass loss observed up to 165°C can be ascribed to the loss of bulk mercury (Hg electrodeposited on Hg). The quantity of mercury lost in this step corresponds to ca. 65.8% of the total electrodeposited mercury. The second mass loss step occurring between 165 and 190°C was attributed to the mercury elimination from the metallic mercury film adhered on the surface by long-range attractive forces (due to London–Van der Waals forces, dipole moments, and coulombic forces) which also

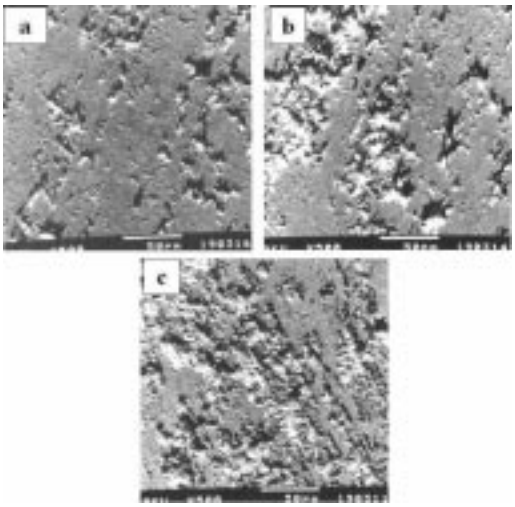

Fig. 2 SEM images of the Ir surface after Hg electrodeposition and heating up to: a – 190°C; magnification: 500×; b – 300°C; magnification: 500×; c – 800°C; magnification: 500×. Electron beam acceleration: 30 kV

exist at the interface. In this step the mass loss corresponds to about 28.7% of the total electrodeposited mercury on the pure iridium foil. The resulting surface presents no typically mercury metallic surface because bulk mercury was eliminated. Figure 2a shows the SEM image for the iridium surface after mercury electrodeposition and heating up to 190°C, the temperature corresponding to the end of the second consecutive step. No mercury film is observed on the foil, only a considerable surface roughening. However, the presence of mercury on this iridium surface was confirmed by EDX microanalysis (Fig. 3) and surface mapping. It was also observed by EDX that the intensity of the Hg peaks decreased as the temperature increased. In the third step (Fig. 1) the mass loss was approx. 5.56% and can be attributed to the removal of mercury present as solid solution. This step was observed between 190 and 500°C and corresponds to a very slow process.

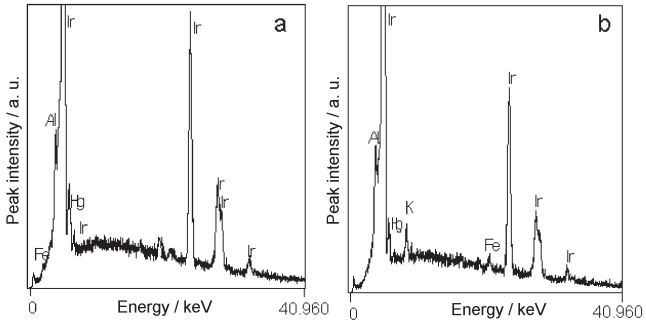

Fig. 3 EDX microanalysis of the Ir foil surface after Hg electrodeposition and heating up to: a – *T*=190°C; VFS: 2048; b – *T*=550°C; VFS: 4096. Electron beam acceleration: 20 kV. Sample time: 300 s

Figure 4 shows the cyclic voltammograms recorded at 50 mV s^{-1} during the electrodeposition of mercury, cathodic scan starting at 0.50 V, and the redissolution, anodic scan, recorded for different $E_{\lambda c}$ (Fig. 4a) and $E_{\lambda a}$ (Fig. 4b). The following anodic current peaks were observed at about 0.2 V (peak C), 0.4 V (peak D), 0.5 V (peak E); and cathodic current peaks at about 0.3 V (peak A) and 0.18 V (peak B). Peak C was assigned to the bulk mercury removal [8, 10–12] and continues to increase as $E_{\lambda c}$ becomes more cathodic. Peaks A and D can be ascribed to the UPD (underpotential deposition) of mercury on iridium and its dissolution, respectively. Peak D seems to increase slightly when the mercury deposition increases, but eventually reaches a limit. The presence of peak B was explained considering the existence of long-range attractive interactions due to London–Van der Waals forces, dipole moments, and coulombic forces at the Ir–Hg interface [10].

The species formed at peaks C and D refer to the oxidation of the Hg(0) to Hg(I). Similarly, in the first two consecutive TG mass loss step metallic mercury is eliminated as mercury vapour. Then, the thermal and the electrochemical processes produce the same effect, i.e. the removal of Hg(0) from the Ir surface.

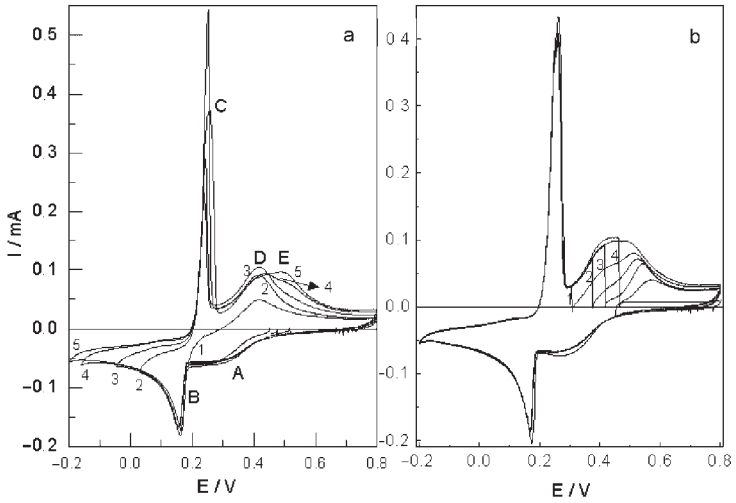

Fig. 4 Cyclic voltammograms of Ir in 1.00 M KNO_3+1.40·10^{-3} M $Hg_2(NO_3)_2$+0.5% HNO_3 (pH 1) deaerated solution, at 25 mV s^{-1} and 25°C. E/(Ag/AgCl/$KNO_{3\ sat.}$). Mercury electrodeposition, cathodic scan beginning at +0.5 V, and redissolution, anodic scan, a – cathodic switching potentials ($E_{\lambda c}$): (1) 180 mV; (2) 70 mV; (3) –50 mV; (4) –160 mV; (5) –200 mV, b – anodic switching potentials ($E_{\lambda a}$): (1) 310 mV; (2) 370 mV; (3) 420 mV; (4) 450 mV; $E_{\lambda a}$, was held until achieve I=0 A

On the other hand, peak E has not been mentioned in the specialized literature [11]. As peak D, peak E reaches a limit value for $E_{\lambda c}$= –0.20 V. In Fig. 4b, the potential was held at each $E_{\lambda\alpha}$ till a null current value was achieved and only after this the scan was restarted. These voltammograms confirm the existence of peak E and its independence of peak D.

As described above long-range attractive interactions can provide stable mercury film formation in cases where no mercury-substrate reaction and/or solvation occur. In this sense, peak E showed in the cyclic voltammograms would be absent. The presence of this peak can be related with the third mass loss step of the TG curve, which was associated with the removal of mercury present as solid solution. Figures 2b, 2c and 2d depict the SEM images of iridium surface after mercury electrodeposition and after heating up to 300 and 800°C (the last temperatures corresponding to the end of the third mass loss step). This set of SEM images shows an increase in the surface roughness as the heating temperature increases up to 800°C. Mercury was also detected by EDX microanalysis and mapping surface on the surface of the foils even when the samples were heated at 300°C. This increase in the roughness for Ir after bulk mercury removal by stripping was also demonstrated using AFM and Auger SEM analysis [9].

According to literature [8, 10], iridium does not react with Hg to form intermetallic compounds. However, the results obtained in the present work suggest that Ir interacts with mercury. In order to identify a possible product of this interaction

X-ray diffraction patterns were obtained for samples heated up to the end of the second mass loss step in the TG curve. The resulting X-ray diffraction data obtained after heating up to 190°C are shown in Table 1 and indicate that the diffraction lines correspond to mercury and iridium substrate. The absence of any diffraction peaks from another phase of Ir–Hg corroborates the low reactivity of iridium with mercury [10, 11]. On the other hand, these results suggest the presence of mercury in the subsurface.

Table 1 Identification of the diffraction peaks obtained on the Ir foil surface heated at 190°C. $K\alpha_{Cu}$=1.54184 Å, step=0.05°, 4≤2θ≤120°. Ir and Hg theoretical values of *d*-spacing was obtained of an Ir prototype [13]

2θ	$d_{cal.}$	$d_{exp.}$	Element
45.03	2.0025	2.0132	Hg
69.18	1.3574	1.3578	Ir
88.03	1.1091	1.1095	Hg
47.45	1.9197	1.9160	Ir
31.65	2.8250	2.8269	Hg
79.29	1.2070	1.2083	Hg
40.74	2.2167	2.2147	Ir
107.08	0.9599	0.9585	Ir
65.66	1.4160	1.4219	Hg
83.52	1.1576	1.1575	Ir
104.49	0.9702	0.9750	Hg
118.40	0.8956	0.8975	Hg
100.65	1.0013	1.0016	Hg
109.63	0.9430	0.9432	Hg

The mapping of Hg distribution on Ir surface foil after Hg electrodeposition and heating up to 190°C, corresponding to the end of the second mass loss step, and heating up to 300°C, corresponding to an intermediate temperature during the last step in the TG curve revealed a homogeneous mercury distribution. It was verified when the samples were heated in the interval from 190 to 300°C, since up to 190°C only bulk mercury was removed. This observation is in agreement with the EDX and X-ray diffraction results obtained in the same temperature range. This behavior has been attributed to an amalgam formation involving mercury diffusion into the lattice of the alloy. According to literature [4, 8], the mercury oxidation present in the substrate of $Pt–Ir_{(20\ mass\%)}$ as a solid solution produces an anodic current peak near the oxygen evolution. In the same way, the mercury identified in the lattice of pure iridium could be answerable for peak E (Fig. 4).

Conclusions

The results obtained in this work allowed to identify mercury film formation on pure iridium foil. This film can be formed by mercury electrodeposition on the metal foil, followed by heating at different temperatures or during the anodic scan in potentials >0.25 V. Mercury desorption occurs in at least three steps, as observed in TG curves and in cyclic voltammetry experiments. SEM images for samples heated between 190 and 800°C indicated an increase in the surface roughness as the mercury was removed from the lattice.

* * *

FAPESP (Fundação de Amparo à Pesquisa do Estado de São Paulo) and CNPq/PIBIC (Conselho Nacional de Desenvolvimento Científico e Tecnológico/Programa Institucional de Bolsas de Iniciação Científica) are acknowledged for the financial support.

References

1 F. L. Fertonani, A. V. Benedetti and M. Ionashiro, Thermochim. Acta, 265 (1995) 151.
2 F. L. Fertonani, M. Ionashiro, P. Melnikov, F. Sanz and A. V. Benedetti, Proceedings of XII Congreso Iberoamericano y IX Encontro Venezolano de Electroquimica, Merida, Venezuela, (1996) 416.
3 E. Milaré, F. L. Fertonani, M. Ionashiro, A. V. Benedetti and P. Melnikov, Proceedings of XIII Congreso de la Sociedad Iberoamericana de Electroquimica, Viña del Mar (1998) 140.
4 F. L. Fertonani, A. V. Benedetti, J. Servat, J. Portillo and F. Sanz, Thin Solid Films, 1 (1999) 341.
5 E. Milaré, F. L. Fertonani, M. Ionashiro and A. V. Benedetti, J. Therm. Anal. Cal., 59 (2000) 617.
6 R. W. Joyner and E. S. Shapiro, Catalysis Letter, 9 (1991) 239.
7 M. Barlow and P. J. Planting, Z. Metallkd, 60 (1969) 292.
8 C. Wechter and J. Osteryoung, Anal. Chem. Acta, 234 (1990) 275.
9 M. A. Nolan and S. P. Kounaves, J. Electroanal. Chem., 453 (1998) 39.
10 S. P. Kounaves and J. Buffle, J. Electroanal Chem., 216 (1987) 53.
11 S. P. Kounaves and J. Buffle, J. Electrochem. Soc., 133 (1986) 2495.
12 E. B. T. Tay, S. B. Khoo and S. W. Loh, Analyst, 114 (1989) 1039.
13 Powder Diffraction File PDF2, Data Base Sets 1-44, published by the Joint Committee on Powder Diffraction Standard – International Centre for Diffraction Data, Pennsylvania, 1988 (CD-ROM).